Received: 14 May 2023 | Accepted: 14 July 2023

DOI: 10.1002/bio.4560

RESEARCH ARTICLE

LUMINESCENCE WILEY
The Journal of Biological and Chemical Luminescence

Orange-red luminescence of samarium-doped bismuth–germanium–borate glass for light-emitting devices

Netheti V. S. Bhagavan[1] | R. Ravanamma[2] | Kummara Venkata Krishnaiah[2] | N. Ravi[2] | Upendra Kumar Kagola[3] | C. R. Kesavulu[4] | P. L. Saranya[5] | V. Venkatramu[6]

[1]Department of Physics, Dr. V.S. Krishna Govt. Degree College (A), Vishakapatnam, Andhra Pradesh, India

[2]Department of Physics, Rajeev Gandhi Memorial College of Engineering and Technology, Nandyal, Andhra Pradesh, India

[3]Department of Physics, School of Applied Sciences, REVA University, Bengaluru, Karnataka, India

[4]Department of Physics, Institute of Aeronautical Engineering, Hyderabad, Telangana, India

[5]Department of Physics, Govt. Degree College for Women, Vishakapatnam, Andhra Pradesh, India

[6]Department of Physics, Krishna University Dr M.R. Appa Row College of PG Studies, Nuzvid, Andhra Pradesh, India

Correspondence
Kummara Venkata Krishnaiah, Department of Physics, Rajeev Gandhi Memorial College of Engineering and Technology, Nandyal, AP, 518501, India.
Email: kvkphd84@gmail.com

Funding information
Science Engineering Research Board, New Delhi, Grant/Award Number: EMR/2017/000009

Abstract

Samarium (Sm^{3+})-doped glass has sparked a rising interest in demonstrating a noticeable emission in the range of 400–700, which is advantageous in solid-state lasers in the visible region, colour displays, undersea communication, and optical memory devices. This study reports the fabrication of Sm^{3+}-doped bismuth–germanium–borate glasses were established using a standard melt-quenching technique and inspection by absorption, steady-state luminescence, and transient studies. The typical peaks of Sm^{3+} ions were detected in the visible range under 403 nm excitation. A strong emission band was detected at 599 nm that resembles the $^4G_{5/2} \rightarrow {}^6H_{7/2}$ transition of Sm^{3+} ions for $BGBiNYSm_{0.5}$ glass. Furthermore, a reddish-orange (coral) luminescence at 646 nm that resembles the $^4G_{5/2} \rightarrow {}^6H_{9/2}$ transition was also perceived. The stimulated emission cross-section of $^4G_{5/2}$ level for $BGBiNYSm_{0.5}$ glass was 0.39×10^{-22} cm^2. Lifetime of the $^4G_{5/2}$ level was enhanced for the $BGBiNYSm_{0.5}$ glass and decreased with an increase in active ion concentrations. The lifetime quenching of ions at the metastable state was because of energy transfer among Sm^{3+} ions by cross-relaxation channels. Commission Internationale de l'Éclairage (CIE) coordinates were evaluated from the emission spectra. Moreover, all the findings recommend these glass as light-emitting materials in the coral region at 599 nm for solid-state lighting applications.

KEYWORDS
coral emission, decay curves, germanium–borate glass, photoluminescence, radiative parameters, Sm^{3+} ion

1 | INTRODUCTION

Lanthanide (Ln)-doped glass has been found as a potential material for the development of lasers [1], amplifiers [2], colour displays [3], memory devices [4], sensors [5], upconverters [6], downconverter [7], optical waveguides [8], and laser cooling of solids [9–11] due to their interesting physical, chemical, mechanical, and optical properties.

Bismuth oxide (Bi_2O_3) is one of the essential prominent glass-forming and fluxing materials. Glass melts with high content of Bi_2O_3 display somewhat high thickness and are prone to form glass. Interest in borate glass is mostly because of compatibility with Ln ions and transition metal ions, low melting temperatures, wide glass-forming ability and high optical nonlinearity [12]. Conversely, boric oxide (B_2O_3) has a long bond length, and a smaller heat of fusion and cation. It is a candidate for a glass former and a flux material. When Bi^{3+} is bonded with oxygen is simply able to form a glass structure. The Bi^{3+} has a high density and is transparent, but it does not form a glass structure itself. Therefore, the glass scintillator is fashioned with B_2O_3

in amalgamation with Bi_2O_3. Recently, bismuth–borate glass has garnered attention due to their conceivable usage in diverse applications that includes thermomechanical sensors, optoelectronic devices, radiation-shielding purposes, reflecting windows, etc. [13]. The combination of two matrix-forming oxides (Bi_2O_3 and B_2O_3) has influenced the glass structure of both the ions with multiple coordination such as BO_4, BO_3, BiO_3 and BiO_6. Moreover, the ability of the structural groups of boron (orthoborate $[BO_3]^{3-}$ and metaborate $[BO_2]^{-}$) as well as the bismuth polyhedron has been extended for forming independent interrelated networks [14].

Bismuth–borate glass exhibits some interesting properties that include low melting temperature in the range of 600–800°C [15], wide glass-forming region, high index of refractive index (1.9–2.3), high mechanical strength, and high chemical durability. Nd^{3+}, Sm^{3+}, Yb^{3+}, and Er^{3+}-doped glasses have been described and observed as possible laser and amplifier gain media. Conversely, bismuth–germanium–borate glass possesses combined properties of germanium and bismuth. Heavy metal ions such as Bi_2O_3, Y_2O_3, and GeO_2 were added to the borate matrix, B_2O_3–Bi_2O_3–GeO_2-Y_2O_3–Na_2O, for enhancing the mechanical strength and chemical durability, ultimately could decrease the host phonon energy.

Samarium (Sm^{3+}) ion is one of the stimulating ions used for investigating the spectroscopic properties due to the $^4G_{5/2}$ level that allows a high stimulated emission and quantum yield. Moreover, Sm^{3+} is a crucial ion as it evidences the emission of green, coral and near-infrared corresponds to the transitions of excited to ground levels, $^6G_{5/2} \rightarrow {}^6H_J$ (J = 5/2, 7/2, 9/2, 11/2). An energy gap of ~7000 cm^{-1} between the metastable state, $^4G_{5/2}$ and the lower state of Sm^{3+} ion does not become embellished due to phonon losses and the orange emission due to the $^4G_{5/2} \rightarrow {}^6H_{7/2}$ transition is barely influenced by a host lattice matrix. It is noteworthy that the nonappearance of lower-lying excited states in Sm^{3+}:materials make them suitable material for applications in photonics. Sm^{3+}-doped glass and complexes were proposed to be suitable in the field of visible solid-state lasers, submarine communication, display devices and optical memory devices [16–19]. In addition, Sm^{3+} emits photons through other channels in the visible region [20–23]. This can be exploited in the exciting field of photonics, such as LED and display technologies. Multicolour emission of Sm^{3+} ions has benefited tunable laser and optical amplifier applications [24]. Furthermore, the ionic state of Sm^{3+} ions can be straightforwardly reduced to the Sm^{2+} state under a reducing atmosphere [25], ionization [26], or irradiation of ultrafast lasers [27] and spectral hole scorching studies [28]. But, less attention has been paid by researchers to a systematic analysis of heavy metal oxide-modified Sm^{3+}-doped borate glass [29–47] related to the other Ln^{3+} ions because of intense emissions. It is utilized definitely for the combination of other Ln^{3+} ions for improving the luminescence quantum efficiency, which is important in the field of optoelectronics [48, 49].

In this work, various concentrations of Sm^{3+}-doped borate–germanium–bismuth (BGBiNYSm) glasses were synthesized and optical and photoluminescence properties investigated. Optical absorption spectra were utilized for evaluating the Judd–Ofelt (JO) [50, 51] parameters of the Sm^{3+} ions. Some of the radiation properties that included branching ratios, transition probabilities, emission cross-section, and radiative lifetime were evaluated. Lifetimes of the $^4G_{5/2}$ state of Sm^{3+} ions were explored through the analysis of the fluorescence decay profile.

2 | EXPERIMENTAL

2.1 | Glass preparation

Sm^{3+}-doped glass, $(30 - x)B_2O_3 + 20GeO_2 + 20Bi_2O_3 + 20Na_2O + 10Y_2O_3 + xSm_2O_3$, where x = 0.05, 0.1, 0.5, 1.0, 1.5, 2.0, and 2.5 mol% referred as $BGBiNYSm_{0.05}$, $BGBiNYSm_{0.1}$, $BGBiNYSm_{0.5}$, $BGBiNYSm_{1.0}$, $BGBiNYSm_{1.5}$, $BGBiNYSm_{2.0}$ and $BGBiNYSm_{2.5}$, respectively, were synthesized using a typical melt-quenching technique. The glass samples have been labelled as proposed in previous work [52–54]. A batch of 15 g of boric acid (H_3BO_3, 99.5%), bismuth oxide (Bi_2O_3, 99.9%), germanium oxide (GeO_2, 99.9%), yttrium oxide

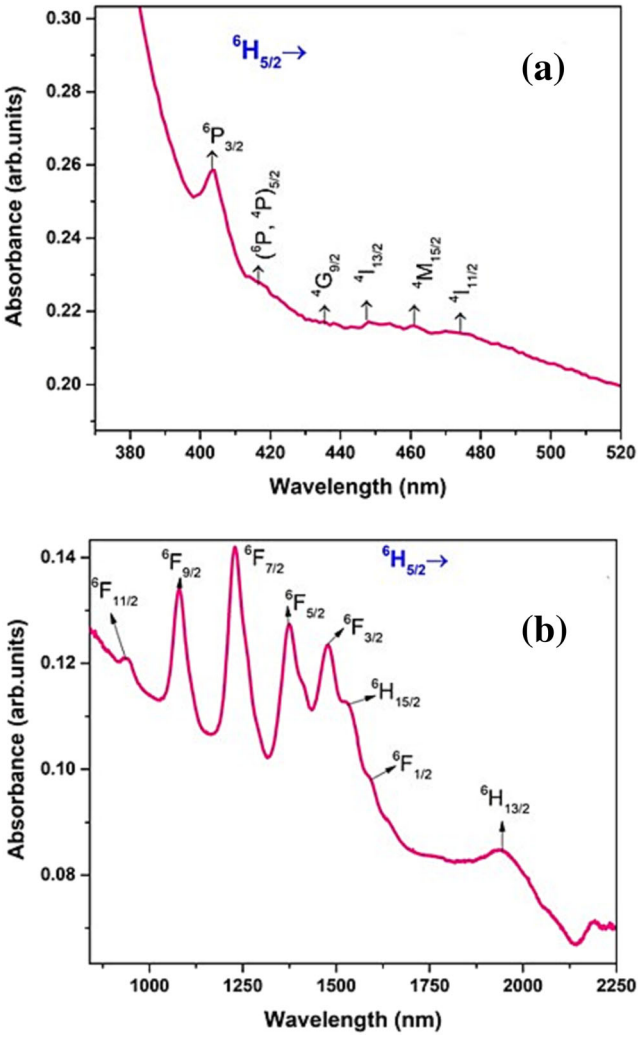

FIGURE 1 Optical absorption spectrum of BGBiNYSm0.5 glass in the (a) UV–visible and (b) NIR regions.

(Y_2O_3, 99.9%) and samarium oxide (Sm_2O_3, 99.9%) was used as starting reagent chemicals without further purification. The weighted composition was ground for 1 h with a mortar and pestle to obtain a homogeneous powder. Well mixed powder was shifted to the alumina crucible (99.9% purity) and heated at 1200°C for 1 h 30 min. Molten glass was cast on the brass mould and preheated at room temperature (RT). This was proximately shifted to an annealing furnace and annealed at 400°C for 2 h to reduce the interior stresses of the glass samples after cooling to RT. Lastly, the samples were refined for further optical characterization.

2.2 | Characterization techniques

Archimedes' principle was adopted to evaluate the density of the glass with water as a dipping liquid. A J.A. Woollam spectroscopic ellipsometer (Model: M-2000VI) was utilized to measure the index of refractive (n). A Varian Cary-5000 ultraviolet (UV)–visible–near-infrared (NIR) optical spectrophotometer (Agilent) was used to record the optical absorption in the range 370–2250 nm. An Edinburg spectrofluorometer (FLS-1000) was utilized to quantify the photoluminescence (PL) spectra. Decay lines were explored by the similar spectrometer upon excitation at a wavelength of 403 nm from a xenon lamp in the pulsed mode.

3 | RESULTS AND DISCUSSION

3.1 | Optical absorption spectrum

The absorption spectrum of $BGBiNYSm_{0.5}$ glass is revealed in Figure 1. Abundant optical bands are entrusted due to different f–f electronic transitions in the wavelengths from 370 to 2250 nm. In total, 14 absorption peaks were revealed in the optical absorption spectra due to 4f electrons that were overlapped by 5s and 5p occupied orbitals. As seen in Figure 1a,b, six optical bands were detected in the visible region and the rest in the NIR region. All evolutions occurred from the lowest state of $^6H_{5/2}$ to accompanying higher states, $^6P_{3/2}$, $(^6P, ^4P)_{5/2}$, $^4G_{9/2}$, $^4I_{13/2}$, $^4M_{15/2}$, $^4I_{11/2} + {}^4I_{9/2}$, $^6F_{11/2}$, $^6F_{9/2}$, $^6F_{7/2}$,$^6F_{5/2}$, $^6F_{3/2}$, $^6H_{15/2}$, $^6F_{1/2}$, $^6H_{13/2}$. The energies of these bands with the corresponding wavelengths are listed in Table 1. The absorption profile revealed that the $^6H_{5/2}\rightarrow{}^6F_{7/2}$, $^6H_{5/2}\rightarrow{}^6P_{3/2}$ and $^6H_{5/2}\rightarrow{}^6F_{9/2}$ evolutions were much stronger related to other evolutions.

All of these optical transitions obeyed the electric-dipole (ED) selection rule, $\Delta J \leq 6$, whereas the $^6H_{5/2}\rightarrow{}^6F_{7/2}$,$^6P_{3/2}$ transitions followed the selection rules of $\Delta J = 0, \pm 1$ relevant to the magnetic-dipole (MD) transition. Among all the revealed optical bands, the $^6H_{5/2}\rightarrow{}^6F_{7/2}$ evolution is said to be an oversensitive transition depending on the Sm^{3+} ion environment.

3.2 | Optical properties: Judd–Ofelt analysis

3.2.1 | Judd–Ofelt (JO) parameters

Judd–Ofelt parameters for $BGBiNYSm_{0.5}$ glass were estimated with the help of the combined area below the absorption peaks and refractive index. The oscillator strengths for both experimental (f_{exp}) and evaluated (f_{cal}) for the transitions were also assessed and listed in Table 1. Furthermore, f_{cal} is related to the ED transition that occurred from the lowest energy state to the higher energy state [49]. Moreover, f_{cal} is evaluated with the help of the least square fitting scheme (Equation 2). The f_{exp} relating to the excited level,$^6H_{5/2}$ is evaluated using Equation (1) [48].

TABLE 1 Oscillator strength (f_{exp} and f_{cal}) of the optical evolutions of Sm^{3+} ions in $BGBiNYSm_{0.5}$ glass.

Wavelength (λ) nm	Energy (ν) cm^{-1}	Transitions from $^6H_{5/2}$	f_{exp}	f_{cal}	$\lvert\Delta f\rvert = \lvert f_{exp} - f_{cal}\rvert$
403	24,813	$^6P_{3/2}$	0.108	0.016	0.092
418	23,923	$(^6P,^4P)_{5/2}$	0.060	0.004	0.056
436	22,935	$^4G_{9/2}$	0.070	0.003	0.066
448	22,321	$^4I_{13/2}$	0.050	0.000	0.049
462	21,645	$^4M_{15/2}$	0.026	0.004	0.021
475	21,052	$^4I_{11/2} + {}^4I_{9/2}$	0.040	0.000	0.040
944	10,593	$^6F_{11/2}$	0.030	0.024	0.005
1,080	9259	$^6F_{9/2}$	0.078	0.145	0.066
1,231	8123	$^6F_{7/2}$	0.221	0.189	0.032
1,372	7288	$^6F_{5/2}$	0.056	0.066	0.009
1,482	6747	$^6F_{3/2}$	0.045	0.052	0.006
1,531	6531	$^6H_{15/2}$	0.033	0.001	0.032
1,592	6281	$^6F_{11/2}$	0.036	0.031	0.005
1943	5146	$^6H_{13/2}$	0.066	0.015	0.050

$\overline{\beta} = 1.0061$
$\delta = -0.0061$
$\delta_{RMS} = 0.046\ (14)$

$$f_{exp} = 4.319 \times 10^{-9} \int \varepsilon(\nu) d\nu. \quad (1)$$

where ϵ is the molar coefficient of extension as a role of wavenumber ν $(cm)^{-1}$. From the JO theory [50, 51], the ED transition intensity was evaluated by intensity parameters Ω_2, Ω_4 and Ω_6:

$$f_{cal} = \frac{8\pi^2 mc\nu}{3h(2J+1)} \frac{(n^2+2)^2}{9n} \chi_{ed} \sum_{\lambda=2,4,6} \Omega_\lambda \left(\Psi J \left\| U^\lambda \right\| \Psi' J'\right)^2 \quad (2)$$

where J represents the total angular momentum of the ground state, n represents the index of refraction of the sample, JO intensity parameters (Ω_λ [$\lambda = 2, 4, 6$]) and $||U^\lambda||$ are the matrix components of the unit tensor operator [55].

The JO variables were predicted and tracked the tendency of $\Omega_6 > \Omega_4 > \Omega_2$ as listed in Table 2 together with other Sm^{3+}:glass [20, 29–47]. Among the JO variables, Ω_2 is highly sensitive to the pre-arrangement of host ions and asymmetric behaviour of the Sm^{3+} ions, whereas the variables Ω_4 and Ω_6 can influence the concentration of Sm^{3+} ions, index of refractive, glass host and photosensitive properties [56]. The Ω_6 value was greater for oxide glass compared with the nonoxide optical glass and in-between for mixed glass. It increased the Sm–O covalent bond due to the existence of nonbridging oxygens within the host matrix [57, 58].

3.2.2 | Photoluminescence excitation (PLE)

Figure 2 shows the PLE spectra of the BGBiNYSm glass measured upon positioning the wavelength at 599 nm. The spectra revealed 13 bands from the lowest level, $^6H_{5/2}$ to various excited levels that include $^4H_{9/2} + {}^4K_{15/2}$, $^4D_{3/2}$, $^4H_{7/2} + {}^6P_{7/2}$, $^4L_{5/2}$, $^6P_{3/2} + {}^4F_{7/2}$, $^6P_{5/2} + {}^4P_{5/2}$, $^4M_{19/2}$, $^4G_{9/2}$, $^4F_{5/2}$, $^4I_{13/2}$, $^4I_{11/2} + {}^4I_{9/2}$, $^4M_{15/2}$, $^4G_{7/2}$ and $^4F_{3/2}$ corresponding to the peak wavelengths at 346, 362, 376, 391, 403, 417, 423, 438, 450, 462, 476, 490, 502 and 527 nm, respectively. Nevertheless, these peaks were not detected well in the optical absorption in the near UV and visible light regions. An intense band at 403 nm was discovered due to the $^6H_{5/2} \rightarrow {}^6P_{3/2}$ evolution and was considered for obtaining the photoluminescence emission of BGBiNYSm glasses. The intensity of the excitation band at 403 nm for the $^6H_{5/2} \rightarrow {}^6P_{3/2}$ transition increased up to $BGBiNYSm_{1.0}$ and later declined with increasing Sm^{3+} ion concentration ($BGBiNYSm_{2.5}$).

TABLE 2 Comparison of JO parameters ($\times 10^{-20}$ cm^2) of Sm^{3+}: $BGBiNYSm_{0.5}$ glass.

Glass matrix	Ω_2	Ω_4	Ω_6	Trend
$BGBiNYSm_{0.5}$ [P.W.]	0.28	0.32	0.48	$\Omega_6 > \Omega_4 > \Omega_2$
BSYCaSm03 [20]	2.90	4.50	4.93	$\Omega_6 > \Omega_4 > \Omega_2$
LFBCdS20 [29]	7.34	5.09	3.70	$\Omega_2 > \Omega_4 > \Omega_6$
ZBSS0.5 [30]	1.56	2.19	1.77	$\Omega_4 > \Omega_6 > \Omega_2$
BCNS1.0 [31]	4.18	8.30	6.38	$\Omega_4 > \Omega_6 > \Omega_2$
PZSMSAg02 [32]	12.69	5.29	4.07	$\Omega_2 > \Omega_4 > \Omega_6$
TNS3 [33]	2.73	0.23	0.17	$\Omega_2 > \Omega_6 > \Omega_4$
LiPbFPS05 [34]	3.79	6.96	3.95	$\Omega_4 > \Omega_6 > \Omega_2$
NNS05 [35]	0.49	6.59	8.89	$\Omega_6 > \Omega_4 > \Omega_2$
MG [44]	0.69	4.06	2.29	$\Omega_4 > \Omega_6 > \Omega_2$
NBOSm10 [45]	0.26	0.50	1.18	$\Omega_6 > \Omega_4 > \Omega_2$
GNS1.0 [46]	3.26	4.75	1.32	$\Omega_4 > \Omega_2 > \Omega_6$
CaAlBSm0.5 [47]	0.49	0.4	0.48	$\Omega_2 > \Omega_6 > \Omega_4$

3.2.3 | Photoluminescence spectra

Figure 3 shows the PL spectra of the BGBiNYSm glasses at different Sm^{3+} ion concentrations upon 403 nm excitation. These glass exposed the emissions at 562, 599, 646, and 713 nm corresponding

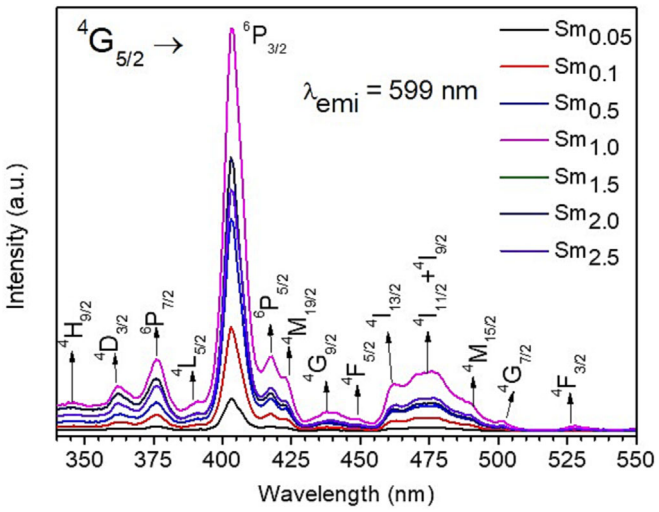

FIGURE 2 Excitation profiles of Sm^{3+}:BGBiNYSm glass upon positioning the emission at 599 nm.

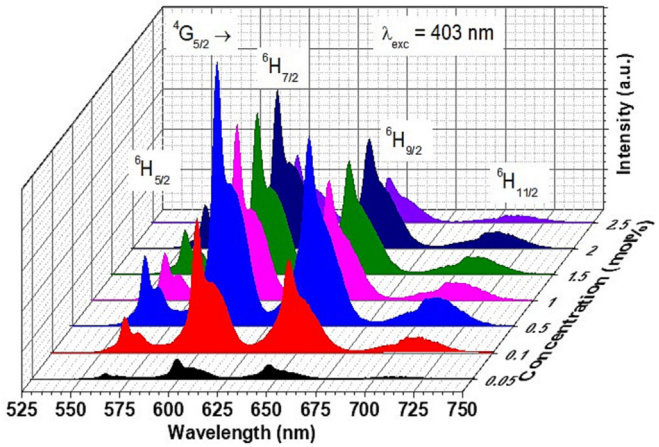

FIGURE 3 Emission spectra of Sm^{3+}:BGBiNYSm glass upon 403 nm excitation.

to the respective evolutions, $^4G_{5/2}\rightarrow{}^6H_{5/2}$, $^6H_{5/2}$, $^6H_{5/2}$, respectively. It was observed that the coral emission at 599 nm for the $^4G_{5/2}\rightarrow{}^6H_{7/2}$ transition increased up to 0.5 mol% and later declined upon increasing Sm^{3+} ion density. This declining luminescence strength was due to the quenching effect through cross-relaxation channels. Therefore, coral emission has many applications particularly for colour displays and light-emitting diodes.

Figure 4 represents the Sm^{3+} ion energy level diagram together with the prominent cross-relaxation networks in BGBiNYSm glass. The resulting combination of cross-relaxation networks is accountable for the quenching of luminescence in these glass:

i. $^4G_{5/2}$: $^6H_{5/2} \leftrightarrow {}^6F_{5/2}$: $^6F_{11/2}$,
ii. $^4G_{5/2}$: $^6H_{5/2} \leftrightarrow {}^6F_{7/2}$: $^6F_{9/2}$,
iii. $^4G_{5/2}$: $^6H_{5/2} \leftrightarrow {}^6F_{9/2}$: $^6F_{7/2}$ and
iv. $^4G_{5/2}$: $^6H_{5/2} \leftrightarrow {}^6F_{11/2}$: $^6F_{5/2}$

Sm^{3+} ions are initially stimulated by the appropriate excitation wavelength. These ions reach beyond the metastable state, $^4G_{5/2}$ and thereafter relax nonradioactively to this luminescence level due to the minor energy gap between the levels. Afterwards, the release of energy arose from the $^4G_{5/2}$ state to the lower energy levels. However, two photoluminescence bands at 599 and 646 nm were attributed due to cracking of Stark's level. The characteristic prominent coral emission was observed principally at 599 nm, which can be beneficial for laser and display applications.

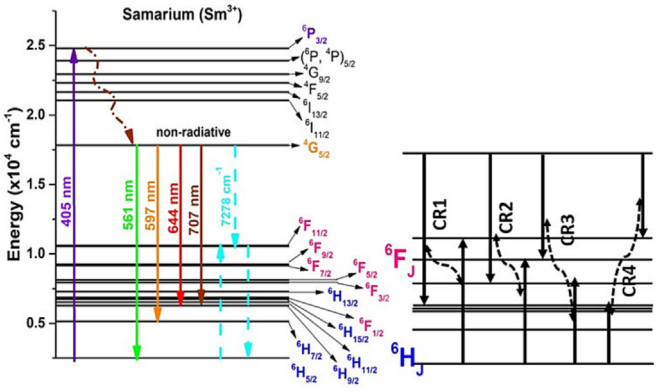

FIGURE 4 Partial energy scheme of the Sm^{3+} ions in BGBiNYSm glass with probable radiative and nonradiative transitions alongside cross-relaxation (CR) channels.

3.2.4 | Luminescence properties

Making use of the JO intensity parameters of the $BGBiNYSm_{0.5}$ glass, the radiative parameters of Sm^{3+} ions that included radiative transition probabilities A_R (s^{-1}), radiative lifetime τ_R (s), and branching ratio β_R were estimated. Table 3 presents the stimulated emission cross-section ($\sigma_{SE} \times 10^{-20}$, cm^2) determined for the $^4G_{5/2}$ level by Equation (3):

$$\sigma SE = (\psi J, \psi' J') = \frac{\lambda_p{}^4 A_R}{8\pi n^2 c \Delta\lambda_{eff}} \quad (3)$$

where λ_p represents the peak emission wavelength, $\Delta\lambda_{eff}$ represents the effective linewidth. σ_{SE} results from the region under the emission peak and its average height, Ln–ligand, ion–ion and ion–ligand interactions that describe the experimental and theoretical results. These are expected for coupled interaction and are characterized by the laser transitions. The σ_{SE} for $^4G_{5/2}\rightarrow{}^6H_{9/2}$ and $^4G_{5/2}\rightarrow{}^6H_{7/2}$ transitions were comparable but differed from the values of $^4G_{5/2}\rightarrow{}^6H_{11/2}$ and $^4G_{5/2}\rightarrow{}^6H_{5/2}$ transitions, as noted in Table 3.

From Table 4, for the $^4G_{5/2}\rightarrow{}^6H_{7/2}$ transition, the radiative lifetime is obtained as high as 5.33 ms for $BGBiNYSm_{0.5}$ glass compared with NNS05 (2.9 ms) [35], 1.68 ms for ZBSS05 [30], BCNS01 (0.61 ms) [31], PZSMSAg02 (0.58 ms) [32], whereas lower lifetimes compared with 5.6 ms for LiPbFPS05 [34] glass. Nevertheless, the τ_{exp} of the $BGBiNYSm_{0.5}$ glass was as high as 1.5 ms and was comparable with 1.87 ms for BSYCaSm03 [20] and 1.94 ms for LiPbFPS05 [34]. Table 4 compares the radiative parameters (A, β_R, τ_R, σ_{SE}, $\Delta\lambda_{eff}$ and σ_{SE} x $\Delta\lambda_{eff}$) for the $^4G_{5/2}$ state of various Sm^{3+}:systems [20, 30–35, 37–39, 41–43].

3.2.5 | Decay curve analysis

Sm^{3+} ion-doped BGBiNYSm glass decay lines of the $^4G_{5/2}\rightarrow{}^6H_{7/2}$ (604 nm) evolution were obtained upon 403 nm excitation and are shown in Figure 5. Single exponential behaviour is reported at lower concentration samples ($BGBiNYSm_{0.5}$) and later on followed a double exponential nature for higher concentration samples ($BGBiNYSm_{2.5}$). The decrease in the lifetime and turning of single to nonexponential behaviour are mainly a result of two processes. The first one is the concentration quenching mechanism at higher concentrations in the $^4G_{5/2}$ state. The second process is nonexponential performance rises

TABLE 3 Radiative parameters of $^4G_{5/2}$ excited level of $BGBiNYSm_{0.5}$ glass.

Transitions from $^4G_{5/2}$	λ_p	$\Delta\lambda_{eff}$ (nm)	A (s^{-1})	τ_R (ms)	σ_{SE} 10^{-22} cm^2	ß		$\sigma_{SE} \times \Delta\lambda_{eff}$ 10^{-28} cm^3
						$ß_{exp}$	$ß_{cal}$	
$^6H_{5/2}$	561	9.46	11.77	8.96	0.08	0.19	0.31	0.75
$^6H_{7/2}$	597	11.59	19.48	5.33	0.39	0.52	0.45	4.52
$^6H_{9/2}$	644	13.01	7.13	14.25	0.26	0.21	0.15	3.38
$^6H_{11/2}$	707	19.68	2.31	43.90	0.02	0.08	0.09	0.39

TABLE 4 Comparison of radiative parameters of BGBiNYSm$_{0.5}$ glass with other reported glass for the $^4G_{5/2}\rightarrow{}^6H_{7/2}$ evolution.

Matrix	A (s^{-1})	β	τ_R (ms)	τ_{exp} (ms)	σ_{SE} 10^{-22} cm^2	($\Delta\lambda_{eff}$, nm)	$\sigma_{SE} \times \Delta\lambda_{eff}$ 10^{-28} cm^3
BGBiNYSm$_{0.5}$ [PW]	11.77	52	5.33	1.5	0.39	11.59	4.52
BSYCaSm03 [20]	164	54	2.70	1.87	11.5	10.28	11.82
ZBSS05 [30]	171	29	1.68	–	14.29	–	–
BCNS1.0 [31]	165	48	0.61	2.48	11.86	9.28	11.00
PZSMSAg02 [32]	471	51	0.58	–	9.66	19.12	18.46
TNS03 [33]	62	39	6.31	–	4.04	–	–
LiPbFPS05 [34]	177	61	5.6	1.94	8.1	–	–
NNS05 [35]	173	50	2.9	2.06	10.02	14.25	14.28
PKAlCFSm01 [37]	174	56	–	1.56	0.98	13.78	1.35
OFBSm01 [38]	101	52	4.9	2.8	5.94	11	6.55
NZLS05 [39]	69	59	8.48	3.72	4.42	13.78	6.09
TWZSm10 [41]	346	46	2.8	0.59	0.77	16.73	1.28
GBNBGSm1.5 [42]	307	58	3.25	1.16	15.59	13.21	20.59
PCfBfTiS20 [43]	9.07	15	1.1	2.42	0.47	17.61	0.82
MG [44]	576	46	–	1.76	2.15	6.45	1.4
NBOSm10 [45]	47.3	68	9.62	1.8	1.66	11.73	–
GNS1.0 [46]	200	36	–	1.81	–	–	–
CaAlBSm0.5 [47]	–	36	–	–	3.96	13.66	5.41

due to the energy transfer (ET) through cross-relaxation (CR) channels of Sm^{3+} ions. Energy exchange among the Sm^{3+} ions is insignificant at low densities but considerably dominant at high concentrations. Consequently, at high concentrations more ET is promising from a spencer-to-collector that guides to a nonexponential nature. A minor fall in the decay curves was noticed because of its nonexponential behaviour as the concentration of Sm^{3+} increases. Dipole–dipole interactions among Sm^{3+} ions are responsible at high concentrations for the behaviour of noncomparable profiles [36, 40]. The lifetime (τ_{exp}) of the noncomparable decay curves was evaluated using Equation (4).

$$\tau_{exp} = \frac{A_1\tau_1^2 + A_2\tau_2^2}{A_1\tau_1 + A_2\tau_2} \tag{4}$$

where A_1 and A_2 represents coefficients τ_1 and τ_2 are decline period for exponential components. Lifetime is assessed from Equation (4) and found to be 1.28, 1.32, 1.68, 0.42, 0.28, 0.24 and 0.21 ms for 0.05, 0.1, 0.5, 1.0, 1.5, 2.0, 2.5 mol% Sm_2O_3-doped glass, respectively. Lifetime rises to 1.5 ms as the Sm^{3+} ion density increases up to 0.5 mol% of the $^4G_{5/2}\rightarrow{}^6H_{7/2}$ evolution for BGBiNYSm glass. Later on, lifetime declines continuously upon raising Sm^{3+} density due to the quenching effect, as displayed in Figure 5. The lifetime of 1.68 ms (BGBiNYSm$_{0.5}$) glass is lower compared with the other investigated glass, 1.76 ms for MG [44], 1.8 ms for NBOSm10 [45], 1.81 ms for GNS1.0 [46], 1.87 ms (BSYCaSm03) [20], 2.06 ms (NNS05) [35], 1.94 ms (LiPbFPS05) [34], 2.65 ms (PKAlCaFSm01) [37], 2.80 ms (OFBSm01) [38], 3.75 ms (NZLS05) [39], 0.59 ms TWZSm10 [41], 1.17 ms for GeBiNaBaGdSm05 [42] and 2.42 ms for PcfBfTiS20 [43] glass.

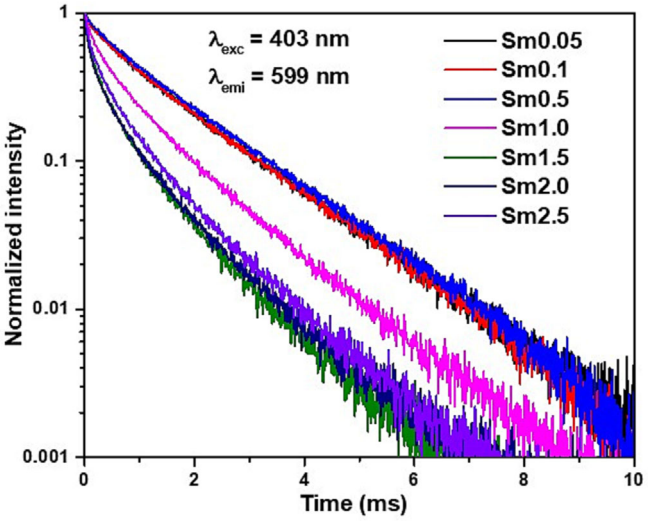

FIGURE 5 Decay profiles of 4G5/2 level with $Sm3^+$ ion concentration variation.

3.2.6 | CIE color coordinates analysis

Emission colour of Sm^{3+}-doped BGBiNYSm glass was inspected with Commission Internationale de l'Éclairage (CIE) 1931 chromaticity diagram. The colour coordinates of CIE (x, y) were estimated according to the procedure described elsewhere [59]. CIE colour coordinates were obtained from the emission spectra of the investigated glass and are shown in Figure 6. The CIE coordinates were (0.60, 0.39), (0.60, 0.39), (0.61, 0.38), (0.60, 0.39), (0.60, 0.38) and (0.60, 0.39) for 0.05,

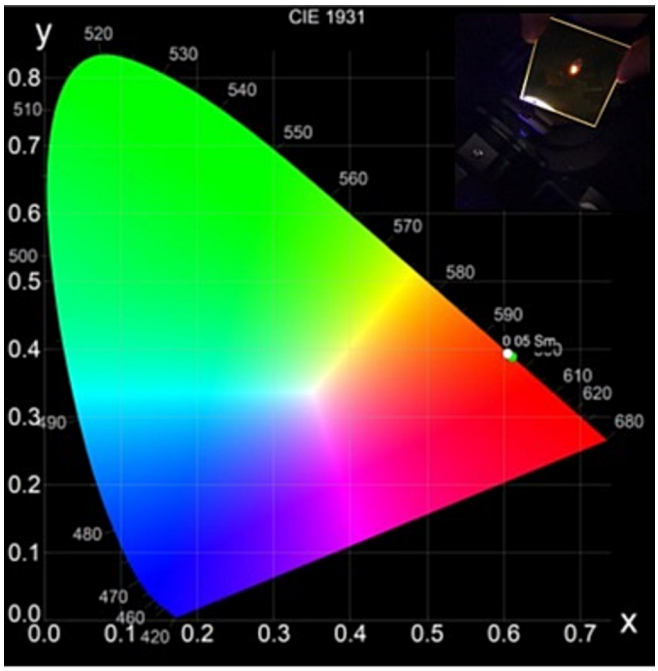

FIGURE 6 CIE coordinates of Sm^{3+}:BGBiNYSm glass under 403 nm excitation. Inset shows the orange-red emission color of the $BGBiNYSm_{0.5}$ glass under 403 nm excitation.

0.1, 0.5, 1.0, 1.5, 2.0, 2.5 mol% Sm_2O_3-doped glass, respectively. These coordinates of glass fell in the orange-red region of the CIE diagram.

4 | CONCLUSION

Sm^{3+} ion-doped bismuth–germanium–borate (BGBiNYSm) glasses were prepared using a typical melt-quenching procedure. From the UV–visible–NIR optical absorption spectrum, based on absorption bands, JO intensity parameters were evaluated. Moreover, the covalency and asymmetry of the BGBiNYSm glass were also presented. The PL profile of Sm^{3+} ions was obtained upon 403 nm excitation. The luminescence profile unveiled an intense band that was noted for the $^4G_{5/2} \rightarrow {}^6H_{7/2}$ evolution at a peak wavelength of 599 nm. Moreover, coral emission was observed to be attributed to the $^4G_{5/2} \rightarrow {}^6H_{9/2}$ evolution at 645 nm. Stimulated emission cross-sections of 0.39×10^{-22} cm^2 and a lifetime of 1.68 ms for $BGBiNYSm_{0.5}$ glass were reported. The PL lifetime of the BGBiNYSm glass demonstrated that the lifetime increased with a rise in the Sm^{3+} density up to 0.5 mol% and later steadily diminished because of concentration quenching. The CIE coordinates were obtained and fell in the orange-red region. These results recommended that the BGBiNYSm glass emitting an orange-red colour could be an appropriate gain medium for solid-state lighting, lasers, and undersea communication applications.

AUTHOR CONTRIBUTIONS

Kummara Venkata Krishnaiah: Conceptualization and supervised the project. Netheti V.S. Bhagavan and R. Ravanamma: Synthesized the samples; curated the data and performed formal analysis. N. Ravi and Upendra Kumar Kagola: Characterization; validation; writing—review and editing. C.R. Kesavulu, P.L. Saranya and V. Venkatramu: Characterization; analysis and draft writing.

ACKNOWLEDGEMENTS

K. Venkata Krishnaiah is grateful to the Science Engineering Research Board, New Delhi for sanctioning a major research project with Number: EMR/2017/000009. K. Upendra Kumar acknowledges the facility support from the "Centre of Excellence in Advanced Materials Research", Department of Physics, School of Applied Sciences, REVA University, Bangalore, Karnataka, India'.

CONFLICT OF INTEREST STATEMENT

The authors declare that they have no known competing financial interests or personal relationships that could have appeared to influence the work reported in this paper.

DATA AVAILABILITY STATEMENT

Not applicable.

ORCID

Kummara Venkata Krishnaiah https://orcid.org/0000-0002-1392-6502

Upendra Kumar Kagola https://orcid.org/0000-0001-9541-3518

REFERENCES

[1] Y. Fujimoto, O. Ishii, M. Yamazaki, *Electron. Lett.* **2010**, *46*, 586.
[2] R. H. Page, K. I. Schaffers, S. A. Payne, W. F. Krupke, *J. Light. Technol.* **1997**, *15*, 786.
[3] C. Zhu, J. Wang, M. Zhang, X. Ren, J. Shen, Y. Yue, *J. Am. Ceram. Soc.* **2014**, *97*, 854.
[4] K. Miura, J. Qiu, S. Fujiwara, S. Sakaguchi, K. Hirao, *Appl. Phys. Lett.* **2002**, *80*, 2263.
[5] K. Linganna, G. L. Agawane, J.-H. In, J. Park, J. H. Choi, *J. Ind. Eng. Chem.* **2018**, *67*, 236.
[6] K. V. Krishnaiah, P. Venkatalakshmamma, C. Basavapoornima, I. R. Martín, K. Soler-Carracedo, M. A. Hernández-Rodríguez, V. Venkatramu, C. K. Jayasankar, *Mater. Chem. Phys.* **2017**, *199*, 67.
[7] I. A. A. Terra, L. J. Borrero-Gonzalez, T. R. Figueredo, J. M. P. Almeida, A. C. Hernandes, L. A. O. Nunes, O. L. Malta, *JOL* **2012**, *132*, 1678.
[8] P. Nandi, G. Jose, C. Jayakrishnan, D. Debbarma, K. Chalapathi, K. Alti, A. K. Dharmadhikari, J. A. Dharmadhikarii, D. Mathur, *Opt. Express* **2006**, *14*, 12145.
[9] E. S. L. de Filho, K. V. Krishnaiah, Y. Ledemi, Y.-J. Yu, Y. Messaddeq, G. Nemova, R. Kashyap, *Opt. Express* **2015**, *23*, 4630.
[10] K. V. Krishnaiah, E. S. L. de Filho, Y. Ledemi, G. Nemova, Y. Messaddeq, R. Kashyap, *Sci. Rep.* **2016**, *6*, 21905.
[11] K. V. Krishnaiah, Y. Ledemi, C. Genevois, E. Veron, X. Sauvage, S. Morency, S. L. de Filho, G. Emova, M. Allix, Y. Messaddeq, R. Kashyap, *Opt. Mater. Express* **2017**, *7*, 1980.
[12] M. Bengisu, *J. Mater. Sci.* **2016**, *51*, 2199.
[13] W. H. Dumbaugh, *Phys. Chem. Glasses* **1978**, *19*(6), 121.
[14] P. Pascuta, G. Borodi, E. Culea, *J. Non Cryst. Solids* **2008**, *354*, 5475.

[15] E. M. Levin, C. L. Mcdaniel, *J Res Natl Bur Stand A Phys Chem.* **1965**, *69A*(3), 237.
[16] F. Ahmadi, A. Asgari, *J. Non Cryst. Solids* **2019**, *505*, 406.
[17] K. S. Rudramamba, D. V. K. Reddy, T. S. Rao, S. K. Taherunnisa, N. Veeraiah, M. R. Reddy, *Opt. Mater.* **2019**, *89*, 68.
[18] J. Fang, H. You, J. Chen, J. Lin, D. Ma, *Inorg. Chem.* **2016**, *45*(9), 3701.
[19] I. I. Kindrat, B. V. Padlyak, B. Kukliński, A. Drzewiecki, V. T. Adamiv, *JOL* **2019**, *213*, 290.
[20] K. Sujita, C. R. Kesavulu, H. J. Kim, J. Kaewkhao, N. Chanthima, Y. Ruangtaweep, *JOL* **2018**, *197*, 76.
[21] I. I. Kindrat, B. V. Padlyak, A. Drzewiecki, *JOL* **2015**, *166*, 264.
[22] V. Thomas, R. G. S. Sofin, M. Allen, H. Thomas, P. R. Biju, G. Jose, N. V. Unnikrishnan, *Spectrochimica Acta Part A: Mol. Bio. Spec.* **2017**, *171*, 144.
[23] V. B. Sreedhar, C. Basavapoornima, C. K. Jayasankar, *J. Rare Earths* **2014**, *32*(10), 918.
[24] J. Yang, B. Zhai, X. Zhao, Z. Wang, H. Lin, *J. Phys. Chem. Solid* **2013**, *74*, 772.
[25] H. Song, T. Hayakawa, M. Nogami, *J. Appl. Phys.* **1999**, *86*, 5619.
[26] E. Malchukovaa, B. Boizot, G. Petitea, D. Ghaleb, *J. Non-Crys. Solids* **2008**, *354*, 3592.
[27] G. J. Park, T. Hayakawa, M. Nogami, *J. Phys. Condens. Matter* **2003**, *15*, 1259.
[28] R. L. Fuller, D. S. McClure, *Phys. Rev. B* **1991**, *43*(1), 27.
[29] Y. C. Ratnakaram, A. Balakrishna, D. Rajesh, M. Seshadri, *J. Mol. Struct.* **2012**, *1028*, 141.
[30] I. Pal, A. Agarwal, S. Sanghi, M. P. Aggarwal, *Spectrochim. Acta Part A: Molec. Bio. Spec.* **2013**, *101*, 74.
[31] I. Arul Rayappan, K. Selvaraju, K. Marimuthu, *Phys. B* **2011**, *406*, 548.
[32] F. Ahmadi, R. Hussin, S. K. Ghoshal, *Opt. Mater.* **2017**, *73*, 268.
[33] S. Q. Mawlud, M. M. Ameen, M. Rahim Sahar, Z. A. S. Mahraz, K. F. Ahmed, *Opt. Mater.* **2017**, *69*, 318.
[34] S. Babu, A. Balakrishna, D. Rajesh, Y. C. Ratnakaram, *Spectrochim. Acta Part A: Molec. Bio. Spec.* **2014**, *122*, 639.
[35] I. Jlassi, S. Mnassri, H. Elhouichet, *JOL* **2018**, *199*, 516.
[36] T. Izumitani, S. A. Payne, *JOL* **1993**, *54*, 337.
[37] S. N. Rasool, L. R. Moorthy, C. K. Jayasankar, *Opt. Commun.* **2013**, *311*, 156.
[38] S. Mahamuda, K. Swapna, M. Venkateswarlu, A. S. Rao, S. L. Shakya, G. V. Prakash, *JOL* **2014**, *154*, 410.
[39] A. Langar, C. Bouzidi, H. Elhouichet, B. Gelloz, M. Férid, *Displays* **2017**, *48*, 61.
[40] R. Vijaya, V. Venkatramu, P. Babu, U. R. Rodríguez-Mendoza, V. Lavín, C. K. Jayasankar, *J. Non Cryst. Solids* **2013**, *365*, 85.
[41] G. Venkataiah, C. K. Jayasankar, K. Venkata Krishnaiah, P. Dharmaiah, N. Vijaya, *Opt. Mater.* **2015**, *40*, 26.
[42] M. Ravi Prakash, G. Neelima, K. Venkata Krishnaiah, N. Ravi, N. Kiran, C. S. Dwaraka Viswanath, T. SubbaRao, V. Venkatramu, *JOL* **2019**, *214*, 116566.
[43] G. Neelima, K. Venkata Krishnaiah, N. Ravi, K. Suresh, S. Nayab Rasool, K. Tyagarajan, T. Jayachandra Prasad, *Mater. Res. Bull.* **2019**, *110*, 223.
[44] H. Liang, X. Liu, J. Tong, P. He, Z. Zhou, Z. Luo, L. Anxian, *Struct. Ceram. Int.* **2023**, *49*, 15266.
[45] I. Ullah, I. Khan, S. K. Shah, S. A. Khattak, M. Shoaib, J. Kaewkhao, T. Ahmad, E. Ahmed, G. Rooh, A. Khan, *JOL* **2021**, *230*, 117700.
[46] Y. Duan, X. Li, R. Shen, Y. Zhang, X. Wang, Z. Guan, K. Wang, Y. Cao, X. Zhang, B. Chen, *Mater. Res. Bull.* **2022**, *153*, 111905.
[47] V. D. Garima, B. G. Hebbar, J. Kaewkhao, N. Intachai, S. Kothan, R. Rajaramakrishna, *Optik* **2022**, *262*, 169366.
[48] C. Bouzidi, M. Ferhi, H. Elhouichet, M. Ferid, *JOL* **2015**, *161*, 448.
[49] L. Li, Y. Wenjun Wang, X. L. Pan, H. M. Noh, J. H. Jeong, *J. Alloys Compd.* **2017**, *723*, 527.
[50] B. R. Judd, *Phys. Rev.* **1962**, *127*, 750.
[51] G. S. Ofelt, *J. Chem. Phys.* **1962**, *37*, 511.
[52] V. Chandrappa, C. Basavapoornima, S. R. Depuru, A. Mohan Babu, C. K. Jayasankar, *J. Non Cryst. Solids* **2022**, *583*, 121466.
[53] P. Ramprasad, C. Basavapoornima, S. R. Depuru, C. K. Jayasankar, *Opt. Mater.* **2022**, *129*, 112482.
[54] K. Udaya Kumar, P. Babu, C. Basavapoornima, R. Praveena, S. R. Depuru, C. K. Jayasankar, *Phys. B* **2022**, *646*, 414327.
[55] C. K. Jayasankar, E. Rukmini, *Opt. Mater.* **1997**, *8*, 193.
[56] C. K. Jorgensen, R. Reisfeld, *J. Less-Common Metals* **1983**, *93*, 107.
[57] I. Ullah, C. S. Sarumaha, A. Angnanon, I. Khan, M. Shoaib, S. A. Khattak, S. Kothan, S. Sangwaranatee, G. Rooh, J. Kaewkhao, *Cer. Inter.* **2023**, *49*, 13774.
[58] J. Zmojda, M. Kochanowicz, P. Miluski, M. Lesniak, M. Sitarz, W. Pisarski, J. Pisarska, D. Dorosz, *J. Mol. Struct.* **2016**, *1126*, 207.
[59] E. Fred Schubert, *Light-Emitting Diodes*, 2nd ed., Cambridge University Press, New York **2006**), Chap. 17 292.

How to cite this article: N. V. S. Bhagavan, R. Ravanamma, K. V. Krishnaiah, N. Ravi, U. K. Kagola, C. R. Kesavulu, P. L. Saranya, V. Venkatramu, *Luminescence* **2023**, 1. https://doi.org/10.1002/bio.4560